nature chemistry

REVIEW ARTICLE

PUBLISHED ONLINE: 23 NOVEMBER 2010 | DOI: 10.1038/NCHEM.907

Graphene oxide as a chemically tunable platform for optical applications

Kian Ping Loh[1]*, Qiaoliang Bao[1], Goki Eda[2] and Manish Chhowalla[2,3]*

Chemically derived graphene oxide (GO) is an atomically thin sheet of graphite that has traditionally served as a precursor for graphene, but is increasingly attracting chemists for its own characteristics. It is covalently decorated with oxygen-containing functional groups — either on the basal plane or at the edges — so that it contains a mixture of sp^2- and sp^3-hybridized carbon atoms. In particular, manipulation of the size, shape and relative fraction of the sp^2-hybridized domains of GO by reduction chemistry provides opportunities for tailoring its optoelectronic properties. For example, as-synthesized GO is insulating but controlled deoxidation leads to an electrically and optically active material that is transparent and conducting. Furthermore, in contrast to pure graphene, GO is fluorescent over a broad range of wavelengths, owing to its heterogeneous electronic structure. In this Review, we highlight the recent advances in optical properties of chemically derived GO, as well as new physical and biological applications.

The exfoliation of graphite oxide — a material first discovered by the Oxford chemist Benjamin Brodie in 1859 — produces atomically thin graphene oxide sheets that are dispersible in basic media[1]. Graphene oxide can be considered as the insulating and disordered analogue of the highly conducting crystalline graphene. The latter has attracted the interest of physicists because of its unique electronic structure with linear dispersion of Dirac electrons. The insulating and defective nature of GO does not allow the observation of fundamental two-dimensional condensed-matter effects, which has limited the interest of physicists in the material. Chemists, however, are increasingly drawn to GO because of its heterogeneous chemical and electronic structures, along with the fact that it can be processed in solution.

The availability of several types of oxygen-containing functional groups on the basal plane and the sheet edge allows GO to interact with a wide range of organic and inorganic materials in non-covalent, covalent and/or ionic manner so that functional hybrids and composites with unusual properties can be readily synthesized (see, for example, recent reviews[2–5] and references therein). Furthermore, GO is an electronically hybrid material that features both conducting π-states from sp^2 carbon sites and a large energy gap (carrier transport gap) between the σ-states of its sp^3-bonded carbons. The tunability of the ratio of the sp^2 and sp^3 fractions by reduction chemistry is a powerful way to tune its bandgap and therefore controllably transform GO from an insulator to a semiconductor and to a graphene-like semi-metal[6]. Although GO can be chemically or thermally reduced to achieve graphene-like properties[7], residual defects such as remnant oxygen atoms[8], Stone–Wales defects (pentagon–heptagon pairs)[9,10] and holes[10] due to loss of carbon (in the form of CO or CO_2) from the basal plane[11] limit the electronic quality — often characterized by carrier mobility — of reduced GO (rGO) compared with its mechanically cleaved counterpart[12,13]. Recent advances in efficient reduction and accounting for screening charges have, however, achieved mobility values in field-effect devices of 5,000 $cm^2\ V^{-1}\ s^{-1}$ (ref. 14).

Owing to these and other unique characteristics, interest among chemists and researchers from other disciplines has increasingly shifted from GO as a precursor of graphene to the properties of GO itself and its possibilities in a wide landscape of applications ranging from plastic electronics, optical materials and solar cells to biosensors. In terms of chemistry, it represents a new type of solution-processable, non-stoichiometric macromolecule that can complex with many organic and inorganic systems.

Structure of GO and rGO

The structure and chemistry of GO have been covered extensively in previous reviews[2,3] and are therefore not described in detail here. However, we shall briefly describe some important features that are crucial for understanding the unique optoelectronic properties of GO and have not been addressed in detail in previous reviews. There is wide variability in the type and coverage of the oxygen-containing functional groups on GO, primarily arising from differences in preparation processes. The functional groups on the basal plane consist mainly of hydroxyls and epoxies. A consequence of the non-uniform coverage by oxygen-containing functional groups of the graphene basal plane is that ordered small (2–3 nm) sp^2 clusters isolated within the sp^3 C–O matrix can be readily observed by Raman spectroscopy[9,15], scanning tunnelling microscopy[16,17], high-resolution transmission electron microscopy[10,18] and transport studies[6,19]. The reduction of GO leads to creation of new sp^2 clusters, through removal of oxygen, which provide percolation pathways between the 2–3-nm sp^2 domains already present. It is notable that the sp^2 domains initially present do not increase in size with reduction. Instead, the newly formed isolated and eventually percolating sp^2 clusters mediate the transport. Because the number of conduction pathways among the newly formed sp^2 clusters is finite, conductance in GO is limited. These sp^2 states can be viewed electronically as the creation of isolated molecular states that aid transport by hopping[6,19] rather than in a ballistic manner as is the case in mechanically exfoliated graphene. Such isolated molecular clusters with finite number of atoms have large bandgaps and provide confinement for electron–hole pairs created by absorption of photons.

From atomic force microscope studies[17,20,21], an individual sheet of GO has a thickness of ~1 nm, which is significantly larger than

[1]Department of Chemistry, National University of Singapore, 3 Science Drive 3, Singapore 117543. [2]Department of Materials, Imperial College London, Exhibition Road, London SW7 2AZ, UK. [3]Department of Materials Science and Engineering, Rutgers University, 607 Taylor Road, Piscataway, New Jersey 08854, USA. *e-mail: chmlohkp@nus.edu.sg; manish1@rci.rutgers.edu

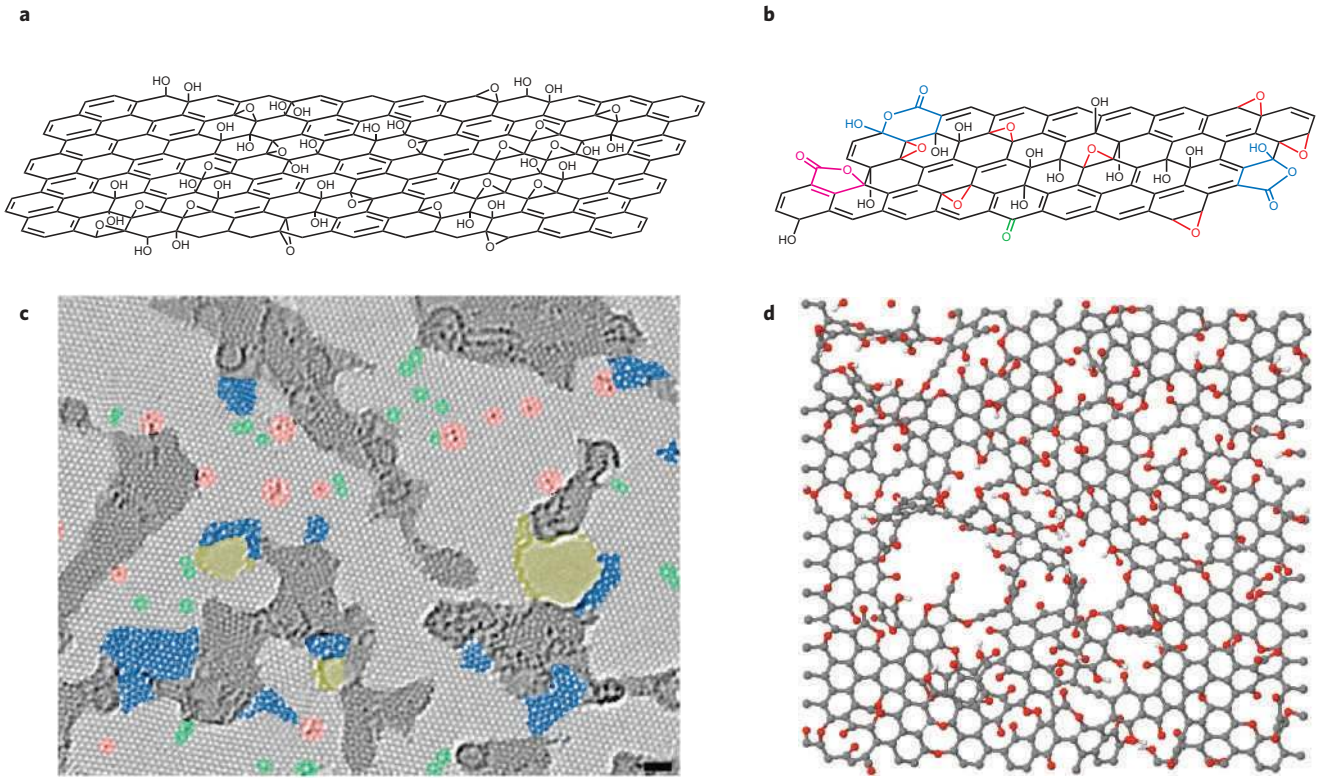

Figure 1 | Chemical and atomic structures of GO and rGO. a, The chemical structure of a single sheet of graphene oxide according to the Lerf–Klinowski model[25,26]. **b**, An updated chemical structure proposed by Gao and colleagues[28]. **c**, Atomic resolution, aberration-corrected high-resolution transmission electron micrograph of a single-layer rGO membrane[10]. Colour scheme highlighting the different structural features: dark grey, contaminated regions; blue, disordered single-layer carbon networks or extended topological defects; red, individual adatoms or substitutions; green, isolated topological defects; yellow, holes and their edge reconstructions. Scale bar: 1 nm. **d**, Atomic model schematically illustrating disordered rGO basal plane consisting of holes, topological defects and remnants of oxygen groups[29]. Figures reproduced with permission from: **a**, ref. 25, © 1998 Elsevier; **b**, ref. 28, © 2009 NPG; **c**, ref. 10, ©2010 ACS; **d**, ref. 29, © 2010 NPG.

that of ideal graphene owing to the presence of oxygen-containing functional groups and adsorbed water above and below the carbon basal plane. The intrinsic thickness of GO sheets (defined here as the interlayer distance in a multilayer stack) is ~0.6 nm, from diffraction studies on dehydrated samples[22]. On the other hand, the lateral dimensions can vary from a few nanometres to hundreds of micrometres[23,24]. Structurally, the Lerf–Klinowski model[25,26] shown in Fig. 1a and experimentally supported by several investigators (see ref. 27 and references therein) represents the widely accepted chemical arrangement of a single atomically thin layer of GO. More recently, Gao and co-workers[28] have proposed a complete structure of GO with five- and six-membered lactol rings decorating the edges as well as esters of tertiary alcohols on the surface (Fig. 1b). A detailed high-resolution transmission electron microscopy study of the defective nature of rGO has recently been reported[9] (Fig. 1c), in which holes, Stone–Wales and other defects have been observed. In contrast with GO, very few calculated models have been proposed for reduced GO. Recently, Bagri *et al.*[29] demonstrated the evolution of the atomic structure of GO as a function of the degree of reduction, using first principles and molecular dynamics calculations. They observed that rGO is disordered, consisting of holes within the basal plane due to the evolution of CO and CO_2 (Fig. 1d) in agreement with the microscopy observations. They also found that residual oxygen (~7–8%) in fully reduced GO is a consequence of the formation of highly stable carbonyl and ether groups that cannot be removed without destroying the graphene basal plane.

The atomic structure of GO is unique in that the graphene basal plane is retained, albeit with large strain. However, as-synthesized GO is primarily a covalent material with ~60% of carbon atoms in the basal plane being sp^3 hybridized through σ-bonding with oxygen in the form of epoxy and hydroxyl groups[26]. An ideal graphene sheet consists entirely of sp^2-hybridized carbon atoms. By contrast, GO is a two-dimensional network consisting of variable sp^2 and sp^3 concentrations, so tuning the sp^2 fraction by careful and controllable removal of specific oxygen groups presents possibilities for tailoring the electrical, optical and/or chemical properties of GO. Because of the non-stoichiometric nature of GO, these properties are dictated by a complex interplay of size, shape and relative fraction of the sp^2 and sp^3 domains.

The presence of defects due to oxygen groups creates chemically reactive sites that allow GO to be cleaved into smaller sheets (that is, unzipped)[30] by chemical or physical means, generating nanosized GO or nanoribbons that have markedly different properties from the micrometre-sized counterpart. For example, it has been demonstrated that GO can be decomposed into small fragments and polyaromatics by sonochemical treatment in acids[31]. Interestingly, such fragments can be reconstituted into fullerenes and carbon wires, demonstrating the very rich chemistry of GO. In other work[32], it has been shown that nanoscale fragments of GO consisting of finite numbers of atoms can be produced by ionic-liquid-assisted electrochemical exfoliation of graphite. Other methods for fabrication of nanosized GO include hydrothermal cleavage of GO to graphene quantum dots in suspension[33].

Transparent conductors with rGO

Reduced GO is highly transparent in the visible spectrum because it is atomically thin. Electronically, rGO is a semi-metal with finite density of states at the Fermi level, similar to disordered mono-[34]

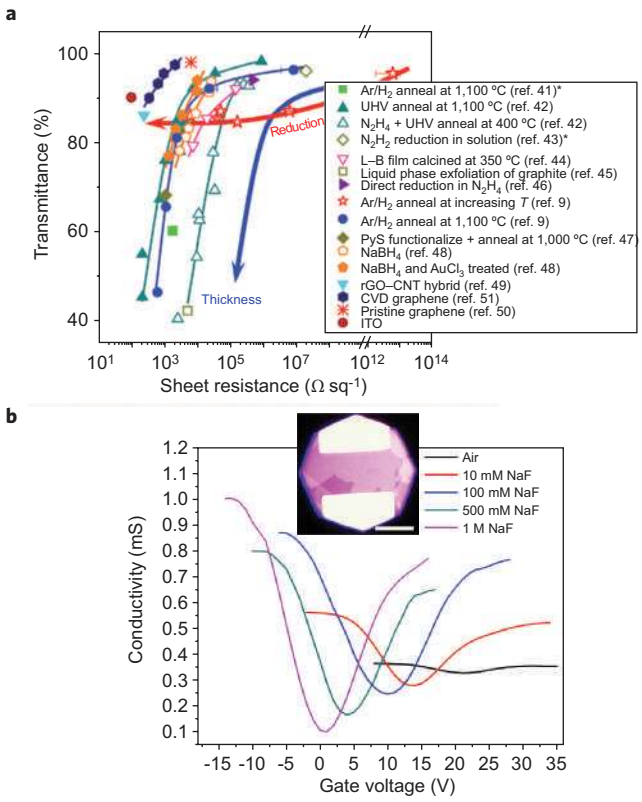

Figure 2 | Optoelectronic and field effect properties of reduced graphene oxide. a, Transmittance at 550 nm versus the sheet resistance of rGO reported in the literature using various reduction methods[9,41–51]. The values from references marked by asterisks were estimated from the information provided. UHV, ultra-high vacuum; ITO, indium tin oxide; L–B, Langmuir–Blodgett; PyS, pyrene-1-sulfonic acid sodium salt. **b**, Transfer characteristics of field-effect devices from laterally large (up to 50 μm) rGO flakes[14]. With increasing ionic strength of NaF, the charge-neutrality point (the voltage at which the conductivity is lowest) shifts towards zero gate voltage, indicating screening of electric fields that originate from charged impurities on the SiO_2 substrate and the nullification of Coulomb scattering. Inset shows the two-probe device consisting of a single-layer rGO flake with large lateral dimensions (scale bar: 20 μm). Figures reproduced with permission from: **a**, ref. 9, © 2009 Wiley; **b**, ref. 14, © 2010 ACS.

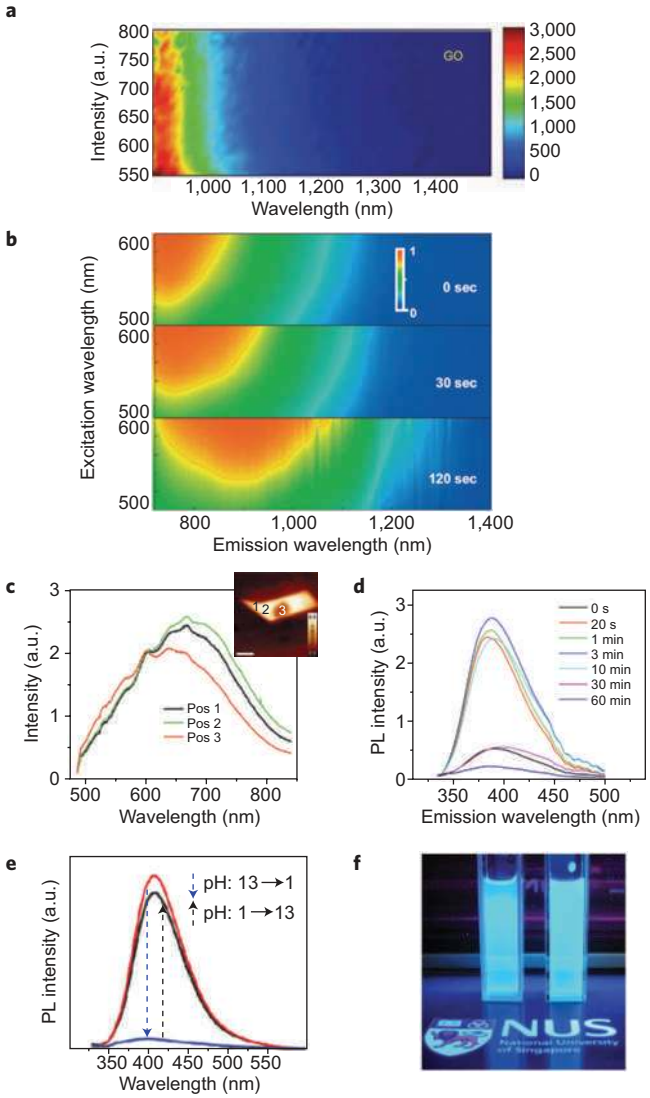

Figure 3 | Fluorescence properties of GO and rGO. a, Fluorescence excitation-emission map of nanosized GO suspension with lateral flake size of 10–300 nm. **b**, Evolution of fluorescence excitation-emission map of GO thin-film samples (average flake size of ~100 μm^2) during hydrazine vapour exposure for 0 to 120 seconds. **c**, Fluorescence from a graphene flake that was oxidized by treating with oxygen plasma; a.u., arbitrary units. Inset shows confocal fluorescence image excited at 473 nm (2.62 eV) for a graphene sample oxidized for 5 s. Scale bar: 10 μm. Colour scale units: kilocounts per second. The spectra were collected at positions (Pos 1–3) marked in the inset. **d**, Fluorescence spectra of a GO thin-film excited at 325 nm after exposure to hydrazine vapour for different periods of time. The fluorescence intensity increases up to 3 mins and then progressively decreases for longer reduction. **e**, The photoluminescence of graphene quantum dots is pH-dependent (from blue to black on increasing the pH and from red to blue on decreasing the pH). **f**, Photograph showing blue fluorescence from supernatant solution of nanosized GO. Figures reproduced with permission from: **a**, ref. 55, © 2008 Springer; **b**, ref. 57, © 2009 AIP; **c**, ref. 70, © 2009 ACS; **d**, ref. 58; © 2010 Wiley; **e**, ref. 33, © 2010 Wiley; **f**, ref. 32, © 2009 ACS.

and multilayered[35] graphene, and shows weak changes in electrical conductance with gate voltage in field-effect devices (on/off ratio <10). Therefore rGO has been widely investigated for transparent conductor applications as a possible replacement for indium tin oxide (ITO)[36] in devices such as organic solar cells[37,38], organic light-emitting diodes[39] and displays (see ref. 40 for a comprehensive review). The optoelectronic properties of rGO in the form of thin films as reported in several publications (ref. 9, 41–49) are summarized in Fig. 2a. We have also included values for mechanically exfoliated graphene[50] and high-temperature chemical-vapour-deposited (CVD) graphene thin-films on copper that were subsequently transferred to glass substrates[51]. The lowest sheet resistance of rGO at transmittance of 80% is ~1 kΩ per square (kΩ sq^{-1}), well above that of ITO and CVD graphene. A recent analysis by the Coleman group reveals that large doping concentrations and high carrier mobilities are simultaneously required to achieve values of ITO with graphene[52]. Various chemical doping schemes involving p- and n-type dopants such as chlorine and nitrogen have been investigated with rGO with limited success. Several devices in which solution processing, mechanical flexibility and electrochemical stability are required have shown exceptional performance with rGO as the transparent and conducting electrode. One example is the incorporation of rGO as the transparent and conducting electrodes in light-emitting electrochemical (LEC) diodes where the high activity of the electrolyte leads to rapid deterioration of ITO, whereas rGO is stable[53].

An alternative pathway for improving the electrical performance of rGO thin-films is to use GO flakes with very large lateral

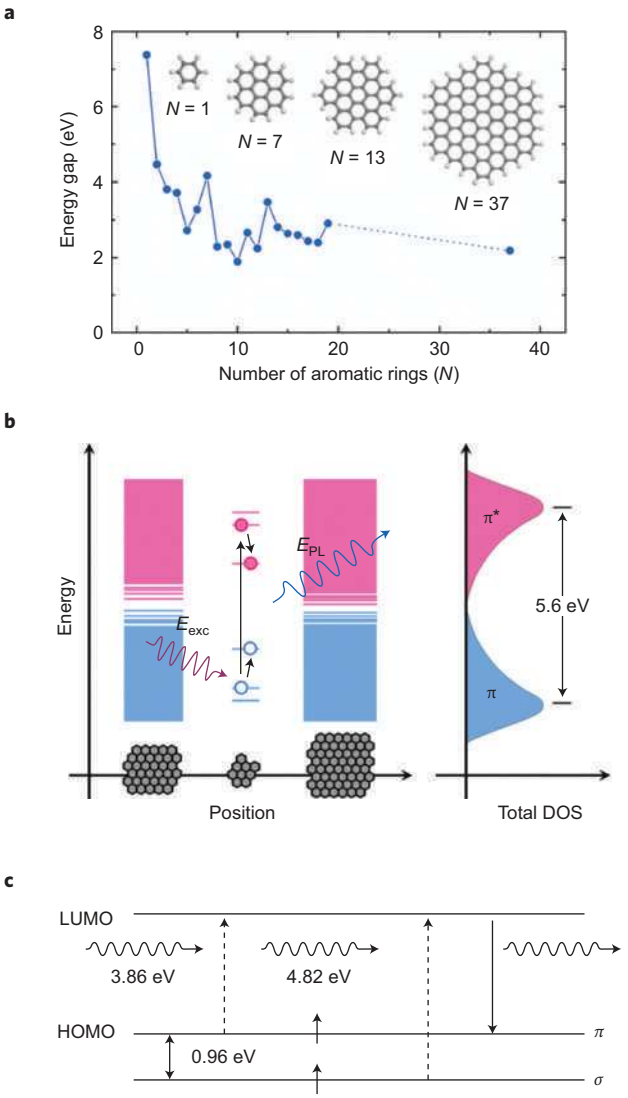

Figure 4 | Electronic structure and fluorescence of GO. a, Calculated energy gap of π–π^* transitions as a function of the number of fused aromatic rings (N). **b**, Schematic band structure of GO (pink and blue represent conduction and valence bands, respectively). Smaller sp^2 domains have a larger energy gap due to a stronger confinement effect. Photogeneration of an electron–hole (e–h) pair on absorption of light (E_{exc}) followed by non-radiative relaxation and radiative recombination resulting in fluorescence (E_{PL}) is depicted. Black arrows denote the transitions of electrons and holes during this process. DOS, electronic density of states. **c**, Schematic of electronic structure at carbene-like zigzag edge site. Dashed and solid arrows indicate electronic transitions associated with excitation and relaxation events, respectively, from the σ- and π-states. Figures reproduced with permission from: **a**,**b** ref. 58, © 2010 Wiley; **c**, ref. 33, © 2010 Wiley.

dimensions (on average more than 25 μm) to minimize the impact of sheet-to-sheet junctions. It has been demonstrated[14] that mobilities of 365 $cm^2\ V^{-1}\ s^{-1}$ for holes and 281 $cm^2\ V^{-1}\ s^{-1}$ for electrons can be achieved in rGO thin films with lateral flake dimensions of ~50 μm, suggesting that the extended π-bonded network can be sufficiently recovered after reduction to allow efficient carrier transport. Furthermore, intrinsic mobility values as high as 5,000 $cm^2\ V^{-1}\ s^{-1}$ have been obtained from solution-processed rGO films when ionic screening is applied to nullify the Coulombic scattering by charged impurities, as shown in Fig. 2b. However, despite the very high mobility values, the three-layered thin films in ref. 14 show sheet resistance values of ~1 kΩ sq^{-1}, comparable to other reports in Fig. 2a.

Fluorescence in GO and rGO

Absence of an energy gap in graphene implies that fluorescence should not be possible unless assisted by phonons[54]. However, in contrast to graphene, the most notable and somewhat unexpected consequence of the heterogeneous atomic and electronic structures of GO and rGO is the observation of near-infrared (NIR), visible and ultraviolet fluorescence[33,55–61]. The intrinsic and tunable fluorescence from GO could open up exciting and previously unforeseen optical applications for graphene-based materials. Although there have been a number of reports on visible and ultraviolet fluorescence from amorphous[62–64] and disordered carbons[65–69], the chemical versatility and tunability of GO combined with solution processability make it attractive for a wide range of applications, as discussed in the following sections. Strongly heterogeneous atomic and electronic structures of GO indicate that fluorescence in GO arises from recombination of electron–hole pairs in localized electronic states originating from various possible configurations, rather than from band-edge transitions as is the case in typical semiconductors. Although the exact mechanisms responsible for fluorescence in GO, especially blue to ultraviolet emission, remain to be elucidated, we summarize some key experimental observations and mechanisms proposed by various groups.

Fluorescence has been observed from GO with a range of lateral dimensions. Low-energy fluorescence in the red to NIR region in laterally nanosized GO aqueous suspensions have been observed by Sun and co-workers[55,56], as shown in Fig. 3a. Luo *et al.*[57] reported comparable fluorescence properties for suspensions and solid samples comprising as-synthesized GO with typical lateral dimensions of 1–10 μm, indicating that the lateral size of the sheets is not the main factor controlling the emission energy. The emission peak was found to redshift towards NIR while diminishing in intensity with progressive reduction treatment by hydrazine vapour exposure (Fig. 3b). Recently, Gokus *et al.*[70] reported broad red to NIR fluorescence from an oxygen-plasma-treated, mechanically exfoliated graphene sample (Fig. 3c). The fact that similar fluorescence properties can be observed in nanosized GO, as-synthesized GO and oxygen-plasma-treated graphene suggests that the origin of this type of emission is closely related.

As-synthesized GO also exhibits weak blue to ultraviolet fluorescence (centred around 390 nm for thin film and 440 nm for solution) when excited with ultraviolet radiation[58,60,61]. The shift in the fluorescence peaks of the suspension and solid sample may be attributed to the differences in the dielectric properties of the surrounding medium, but further work on suspended samples is required to understand the influence of the environment. Eda *et al.*[58] demonstrated that the intensity of as-deposited GO can be greatly increased on short exposure to hydrazine vapour (Fig. 3d). During reduction, little or no peak shift of the blue fluorescence was observed. Optical and electrical measurements on the thin films indicated that maximum fluorescence intensity was achieved when GO was only slightly reduced. Similarly, recent studies have shown that reduction of GO leads to an enhancement or appearance of blue fluorescence while simultaneously quenching the initial low-energy fluorescence centred at yellow to red wavelengths[60,61].

Pan *et al.*[33] demonstrated that the blue fluorescence (Fig. 3e) from a graphene quantum dot is pH-dependent. That is, the fluorescence is strong enough to be observable by the naked eye at high pH levels, whereas it is nearly quenched at low pH conditions. In support of their model, they argue that protonation of the emissive zigzag sites with $\sigma^1\pi^1$ ground state in acidic conditions quenches the fluorescence, whereas deprotonation in alkaline conditions recovers it. Similar blue fluorescence has also been observed in water-soluble

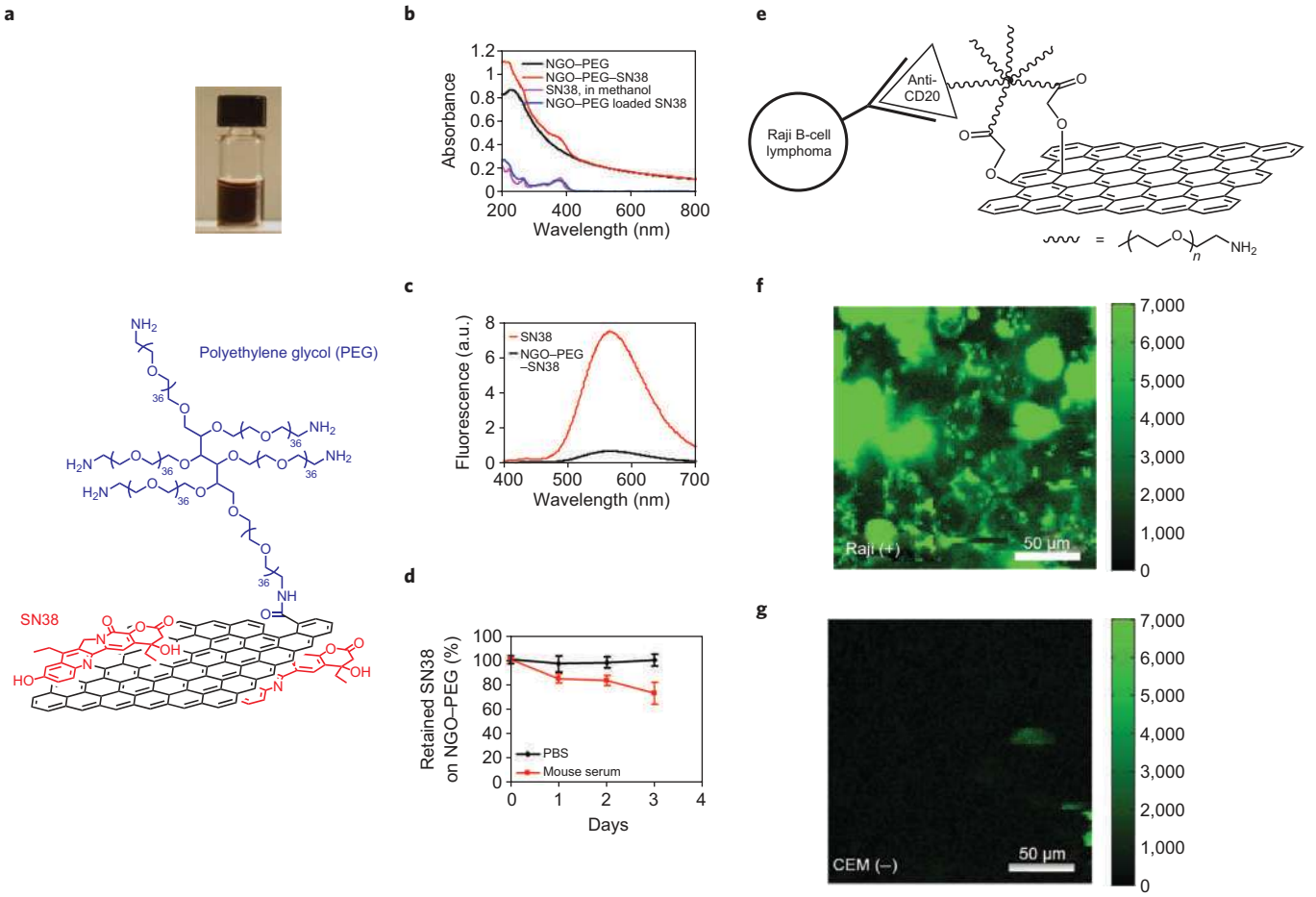

Figure 5 | Fluorescent GO for biological applications. a, Schematic representation illustrating SN38 loading on nanosized GO–PEG by π–π interactions. Inset shows a photo of GO–PEG–SN38 water solution. **b**, Ultraviolet–visible absorption spectra of GO–PEG and GO–PEG–SN38. **c**, Fluorescence spectra of SN38 and GO–PEG–SN38. **d**, Retained SN38 on GO–PEG versus the incubation time in PBS and serum[56]. GO–PEG composite does not show obvious cytotoxicity and could potentially find use in the delivery of anticancer drug SN38 (a potent topoisomerase I inhibitor insoluble in water). **e**, Schematic representation showing that GO–PEG conjugated with anti-CD20 antibody selectively binds to CD20 cell surface receptors on Raji B-cell lymphoma. **f**, **g**, False-coloured green images showing NIR fluorescence of CD20-positive Raji-cells (**f**) and CD20-negative CEM T-cells (**g**), treated with the GO–PEG Rituxan conjugate[55]. Figures reproduced with permission from: **a**–**d**, ref. 56, © 2008 ACS; **e**–**g**, ref. 55, © 2008 Springer.

GO fragments produced by ionic-liquid-assisted electrochemical exfoliation of graphite (Fig. 3f)[32].

The presence of localized finite-sized molecular sp^2 clusters within an sp^3 matrix can lead to confinement of π- electrons in GO. Radiative recombination of electron–hole pairs in such sp^2 clusters can give rise to fluorescence[62–64]. The size of sp^2 clusters determines the local energy gap (Fig. 4a) and therefore the wavelength of the emitted fluorescence. Because a range of sp^2 cluster sizes are present in GO, the collective band structure has no signature features as depicted in Fig. 4b. It can be surmised from Fig. 4a that, for example, emission in the ultraviolet–visible region can occur from sp^2 clusters with sizes of less than 1 nm amounting to ~20 aromatic rings. Larger sp^2 domains (>2 nm) possess smaller gaps, which may account for red to NIR emission. However, the calculations in Fig. 4a are designed to provide only preliminary insight and can be considered simplistic because they do not take into account the influence of the surrounding sp^3 matrix as well as other sp^2 configurations (for example shape, symmetry and topology of the sp^2 chains and clusters) that might be present in GO.

An alternative explanation for fluorescence in GO has been proposed by Pan *et al.*[33] who used the hydrothermal route to cut GO sheets into blue-luminescent graphene quantum dots. Based on their analysis, emission from free zigzag sites with a carbene-like triplet ground state described as $\sigma^1\pi^1$ has been proposed as a possible explanation for the fluorescence (Fig. 4c). Furthermore, previous observations of fluorescence from carbon nanoparticles[66–68] and functionalized carbon nanotubes[65,69] have been attributed to the presence of oxygen-containing functional groups, in a similar way to the mechanism reported for surface-oxidized silicon nanocrystals[71]. However, the observed enhancement of blue fluorescence with reduction suggests that oxygen functional groups can be excluded as the origin[58,60,61]. Instead, the creation of localized sp^2 clusters and structural defects during reduction[6] are more likely to be responsible for the origin and enhancement in blue fluorescence[58].

The fluorescence in GO is tunable between ultraviolet, visible and NIR, and is robust and reproducible with reported quantum efficiency values as high as 6.9% (ref. 46). These features suggest that fluorescence from GO could be readily incorporated in a variety of applications.

Fluorescent GO and rGO for biological applications

The intrinsic fluorescence of GO in the visible and NIR range makes it attractive for numerous applications, and recently several biological applications using the versatile optical properties of GO have emerged. We briefly describe the salient features of these studies to provide insight into how the unique optical properties of GO can be

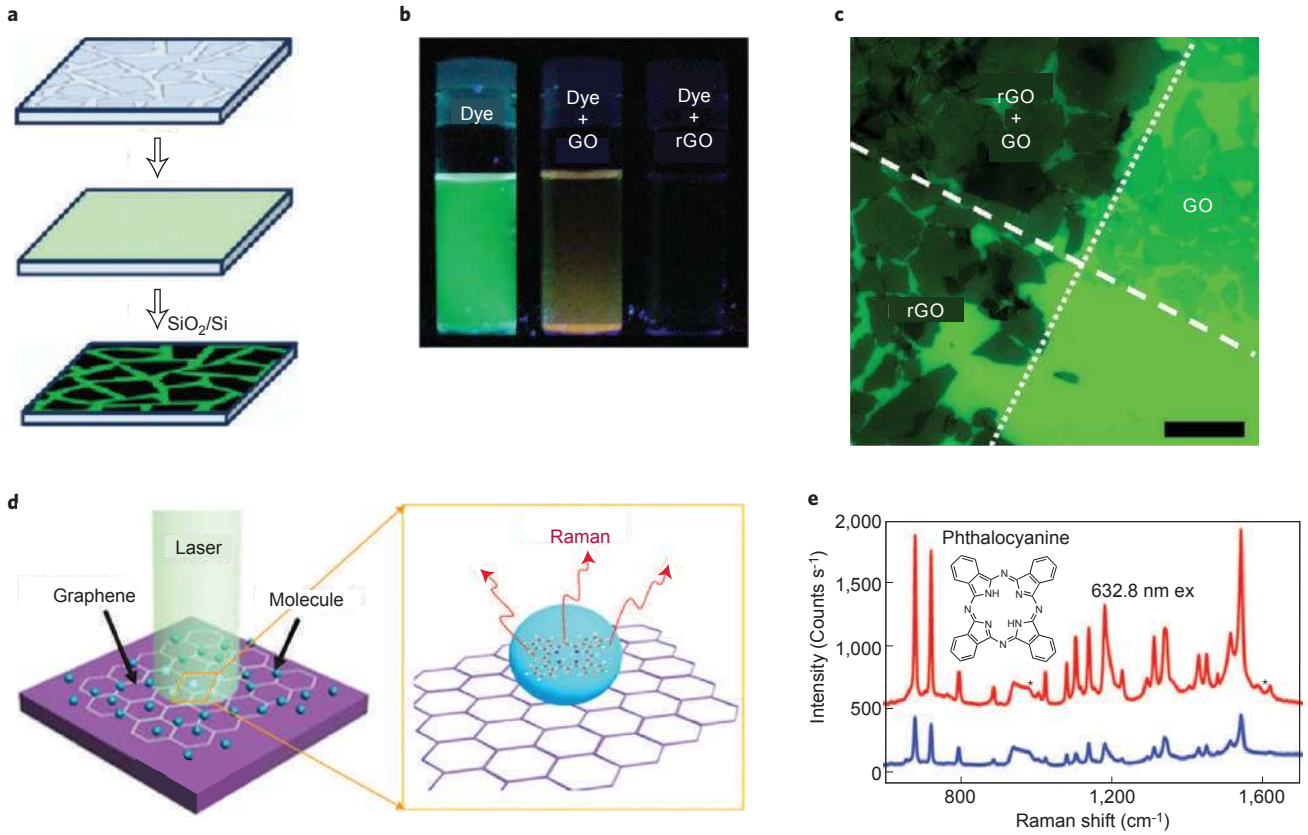

Figure 6 | Fluorescence quenching with GO and rGO and Raman enchancement. a, Visualizing GO and rGO by fluorescence-quenching microscopy. **b**, Photograph showing the quenching effect of GO and reduced GO in a fluorescein solution. **c**, Glass coverslip covered with GO and rGO, showing different quenching efficiency. Scale bar 25 μm. **d**, Schematic showing graphene fluorescence quenching in resonant Raman spectroscopy. **e**, Raman signal of phthalocyanine deposited on graphene (red line) showing enhancement in intensity at an excitation wavelength of 632.8 nm compared with that on SiO_2/Si substrate (blue line) owing to graphene-induced fluorescence quenching. The peaks marked by asterisks indicate the Raman signal from Si (at 960 cm^{-1}) and graphene (at 1,586 cm^{-1}). Inset: the chemical structure of phthalocyanine. Figures reproduced with permission from: **a**–**c**, ref. 76, © 2009 ACS; **d**,**e**, ref. 85, © 2009 ACS.

used. Specifically, applications in drug delivery (Fig. 5a–d) and live cell imaging (Fig. 5e–g) are highlighted[55,56]. From a pure chemistry viewpoint, GO has distinct advantages in biological applications over other related materials such as carbon nanotubes (CNTs). First, it has excellent water solubility without the cutting and de-bundling process required for CNTs. Second, it does not have the oxidative stress originating from metallic catalyst impurities, the latter being a cause of CNT-induced toxicity. Third, it does not require surfactants for dispersion; some of the observed cytotoxicity in CNT has been linked to surfactants[72]. Fourth, it has high specific surface area, which allows for the high-density loading of drugs through electrostatic bonding or π–π cooperative interactions.

Dai and co-workers[55,56] made use of fluorescence from nanosized GO functionalized with polyethylene glycol (PEG) for bio-imaging of live cells. The complexing of GO with the hydrophilic polymer PEG further enhances the water solubility. As has been demonstrated (Fig. 5a–d)[56], such a GO–PEG composite does not show obvious cytotoxicity and can be used for the delivery of water-insoluble cancer drugs (SN38, a potent topoisomerase I inhibitor). For example, GO–PEG covalently conjugated with the B-cell-specific antibody Rituxan (anti-CD20) (Fig. 5e) can selectively recognize and bind to B-cell lymphoma cells, and not to CD20-negative CEM T-cells. The strong NIR fluorescence in Fig. 5f but very weak fluorescence in Fig. 5g demonstrates selective binding of GO–PEG Rituxan conjugate to B-cells.

In vivo fluorescence imaging of GO–PEG revealed surprisingly high uptake in several xenograft tumour mouse models[55,56]. In contrast to PEGylated CNTs, PEGylated GO shows several interesting *in vivo* behaviours including highly efficient tumour passive targeting and relatively low retention in reticuloendothelial systems. The strong optical absorbance of GO in the NIR region has also been applied to *in vivo* photothermal therapy, achieving ultra-efficient tumour ablation after intravenous administration and low-power NIR laser irradiation[73]. Furthermore, on histology and blood chemistry analysis, no obvious toxic effect of PEGylated GO was noted in the injected mice. These results suggest that GO could be promising for biomedical applications such as cancer treatment.

Fluorescence quenching with GO

Interestingly, although GO is itself fluorescent, it can also quench fluorescence. These seemingly contradictory properties are a manifestation of the heterogeneous chemical, atomic and electronic structures of GO. It is well known that graphitic carbon quenches fluorescence from dye molecules adsorbed on its surfaces[74]. In a similar manner, the sp^2 domains within GO and rGO allow quenching of nearby fluorescent species such as dyes[75,76], conjugated polymers[77,78] and quantum dots[79]. The quenching efficiency of GO is significantly improved after reduction[76]. Although quantitative analysis of the quenching efficiency of GO and rGO has yet to be reported, Xie *et al.*[80] recently estimated the quenching efficiency of pristine graphene to be as large as 10^3. Studies indicate that this quenching effect originates from fluorescence (or Förster) resonance energy transfer, or non-radiative dipole–dipole coupling, between the fluorescent species and GO or rGO[76,78,79].

This effect forms the basis of a technique called fluorescence quenching microscopy (FQM) where GO or rGO provide dark contrast compared with the surrounding fluorescent medium[76,81]. With the help of a low-pass optical filter to remove the signal from the excitation source, FQM allows the visualization of morphological features of individual GO and rGO sheets on arbitrary substrates and within liquids (Fig. 6a)[76,81]. FQM significantly enhances the contrast of GO and rGO in comparison with what is commonly achieved with conventional optical imaging techniques that rely on interference effects and require specifically designed substrates[82]. Figure 6b,c shows results from FQM studies[76] of GO using dyes such as red DCM (4-(dicyanomethylene)-2-methyl-6-(4-dimethylaminostyryl)-4H-pyran), green fluorescein and blue BBOT (2,5-bis(5-tert-butyl-2-benzoxazolyl)thiophene). Kim *et al.*[76] demonstrated that GO is able to quench fluorescence from dye molecules separated by a polystyrene spacer layer ~20 nm thick. It is worth noting that the large effective remote quenching distance of GO is close to the theoretically predicted value for pristine graphene (~30 nm)[83,84]. On the basis of such fluorescence quenching effects, graphene has been used as a substrate to suppress fluorescence interference in resonance Raman spectroscopy to produce relative signal enhancement (Fig. 6d and e)[80,85].

Biosensing by fluorescence quenching in GO

The presence of ionic groups and aromatic domains suggests that GO can interact with biomolecules in a number of ways. Ionic groups such as O^- and COO^- that decorate the planes and edges of GO and rGO allow electrostatic interactions with charged proteins and deoxyribonucleic acid (DNA)[86], and the aromatic scaffold provides a platform for π–π stacking and quenching of dyes. Graphene oxide, with its weakly ionizable carboxylic groups, can also be considered as a low-strength acid resin, allowing ion exchange interactions with charged molecules to form molecular complexes. Such interactions suggest that binding strengths of biomolecules are tunable with GO or rGO, affording the possibilities of selective extraction in proteomics.

Towards this end, fluorescence quenching has been used as the basis of GO optical sensors for sensing single-stranded DNA (ssDNA) and biomolecules[79,87,88]. The sensor concept is based on the fluorescence quenching of the dye-labelled ssDNA on binding with GO. More specifically, the dye-labelled probe DNA forms a duplex with the target molecule so that it becomes rigid, and conformational changes release the duplex from GO, reversing the quenching effect. The mechanism is schematically shown in Fig. 7a–c[87]. For example, owing to the strong binding affinity between GO and human thrombin aptamer (5′-TCTCTCAGTCCGTGGTAG GGCAGGTTGGGGTGACT-FAM-3′), the quenching effect reaches an efficiency of 96%. When 100 nM human thrombin is introduced as the target analyte, a significant fluorescence enhancement can be observed[87]. Recently, He *et al.*[88] developed a sensitive and rapid strategy with multicolour DNA analysis, as shown in Fig. 7d–f. The results from the initial studies suggest that it may be possible to extend optical sensing to a wide spectrum of analytes by complementing GO with functional nucleic acid structures.

A GO-based detection platform has several advantages for optical sensing of biomolecules compared with conventional molecular beacons. The intrinsic advantages arise from the unique physical and chemical structure of GO. The two-dimensional sheet is equipped with a range of functional groups that can interact in an ionic, covalent or non-covalent manner, so that in principle it provides the highest extraction efficiencies of biomolecules per unit area of virtually any material. Its effectiveness in quenching fluorescence affords advantages over alternative carbon materials such as nanodiamonds[89,90] and carbon nanotubes[91] that have been investigated for biosensing. It is envisaged that a wide variety of detection protocols based on fluorescence (Förster) resonance energy transfer could be developed on GO platforms, and the exceptional fluorescence-quenching ability should allow optical

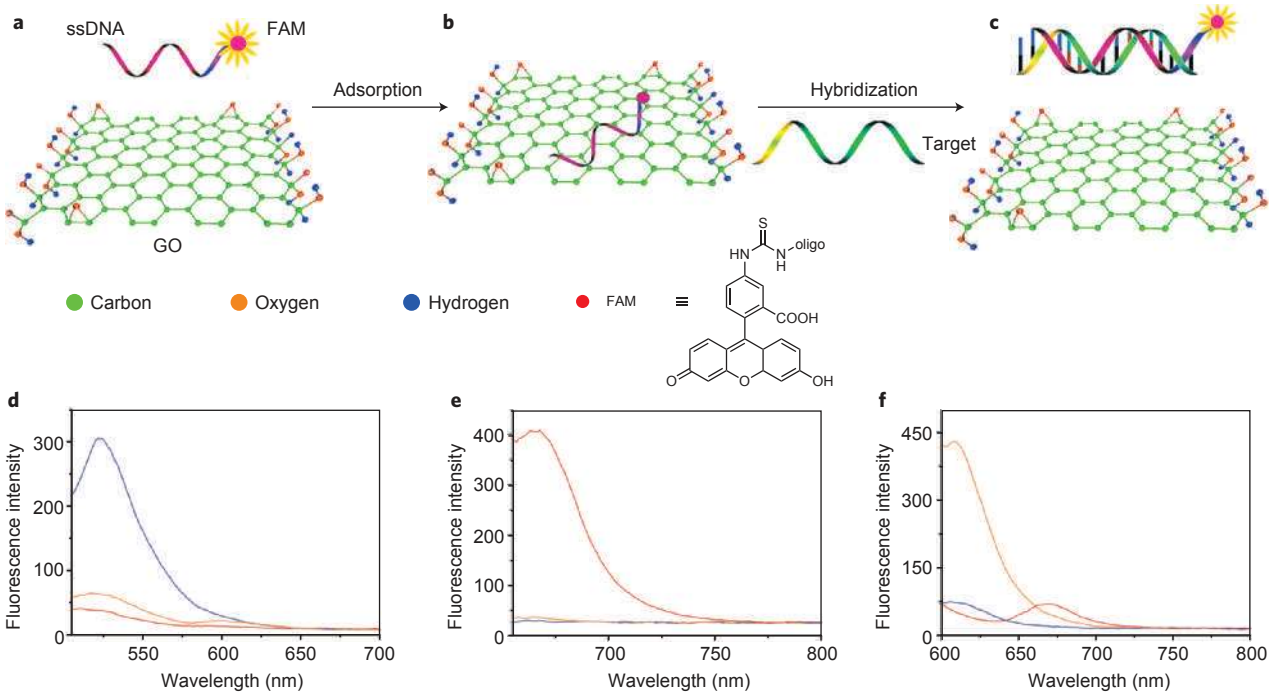

Figure 7 | Biosensing by fluorescence quenching in GO. a–c, Schematic illustrating biosensing based on target-induced fluorescence change of the ssDNA–FAM–GO complex (FAM: fluorescein-based fluorescent dye)[87]. The fluorescence of dye-labelled ssDNA is quenched upon adsorbing onto GO (**b**) and can be restored on being subjected to target molecules (**c**), owing to the conformation change of the dye-labelled DNA. **d–f**, Representative fluorescence spectra[88] on addition of different targets, T5 (blue), T6 (red) and T7 (orange), with excitation/emission wavelengths of 494/526 (**d**), 643/666 (**e**) and 587/609 (**f**) nm/nm. Figures reproduced with permission from: **a–c**, ref. 87, © 2009 Wiley; **d–f**, ref. 88, © 2010 Wiley.

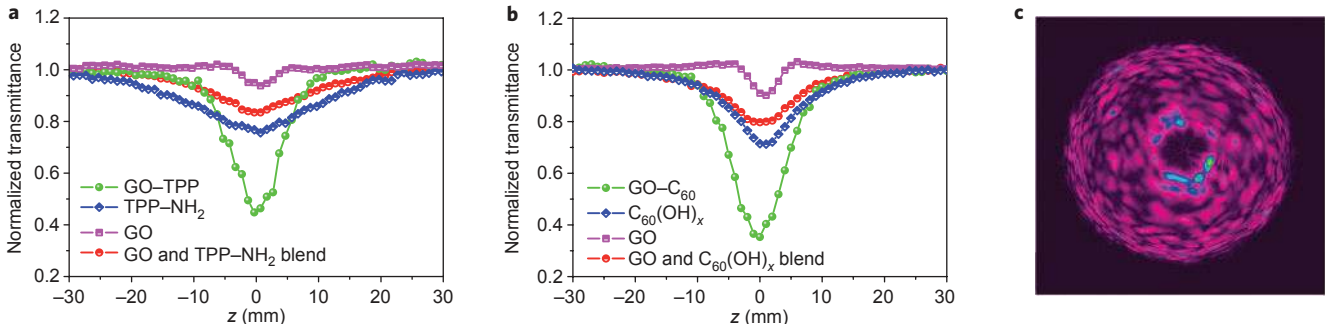

Figure 8 | Nonlinear optical properties of GO and its derivatives. a,**b**, Open-aperture *z*-scan curves of GO–porphyrin (TPP) (**a**) and GO-fullerene (C_{60}) hybrid (**b**). The measurements were carried out at 532 nm with 5-ns pulses, and show that the covalent functionalization of GO with chromospheres (porphyrins and fullerenes) enhances its nonlinear properties. The difference between the two curves corresponding to GO in **a** and **b** arises from the experimental variability between the samples. **c**, Optical image showing strong nonlinear scattering signals for graphene–TPP. Figures reproduced with permission from ref. 96, © 2009 ACS.

detection of organic molecules with a spatial resolution beyond diffraction limits[92]. Finally, its low cost, multiple molecular target detection and high sensitivity suggests that it may emerge as the next-generation optical sensing platform for biomolecules.

Nonlinear optics with GO

Recently, surprising results have been reported on the nonlinear optical properties of graphene[93–97] and their use in ultrafast lasers as saturable absorbers[98,99] (materials in which absorption decreases at high intensity). In principle, GO with a tunable energy gap could surpass the performance of graphene for such applications. Towards this end, we briefly describe some unique nonlinear optical features of GO. For eye protection when observing through an optical sighting system, a broadband optical limiter (an optical component that limits transmission of intense light) is required, covering the entire visible spectrum (and possibly extending into the infrared) with good linear absorption at low input levels. Very few nonlinear optical materials can fulfil these requirements at all laser pulse lengths. The interband optical transitions in graphene are independent of frequency over a wide range and depend only on the fine-structure constant[50], so it is promising as a broadband optical material.

The advantages of GO are its two-dimensional nature and readily functionalizable chemistry, which allow it to be combined with complementary nonlinear optical materials in tandem configurations, or to be hybridized with organic dyes. The broadband nonlinear optical response of graphene and GO dispersions has been studied by several groups[97,100]. Generally, GO shows a better optical limiting response than that of C_{60}, the benchmark material. Liu *et al.*[93] demonstrated that the nonlinear absorption of GO is different from its allotropes such as fullerenes and carbon nanotubes but similar to organic materials. In pure GO, for picosecond pulses two-photon absorption is found to dominate the nonlinear absorption, whereas for nanosecond pulses excited state absorption also influences the nonlinear response. Chen's group improved the optical limiting properties of GO by linking it with nonlinear optical molecules such as porphyrin (TPP)[94], oligothiophene[95] and fullerene (C_{60})[96], as shown in Fig. 8a,b. They found that the nonlinear optical performance in the nanosecond regime is indeed improved by covalent functionalization of GO with chromospheres such as porphyrins and fullerenes. Compared with benchmark fullerene materials, superior optical limiting effects were observed in hybrid GO–dye materials, indicating that a combination of optical limiting mechanisms operate, including nonlinear optical absorption and scattering (Fig. 8c), as well as photoinduced electron or energy transfer in GO–organic hybrids.

Conclusions and outlook

Graphene oxide is often referred to as a disordered material. But it is this inherent disorder, induced by the presence of functional groups, that provides opportunities for tailoring its chemical functionality as well as its optoelectronic properties. The unique chemical structure of GO and rGO along with heterogeneous electronic structure due to the presence of sp^2 and sp^3 bonding confers on them intriguing properties that offer exciting prospects for new applications. The use of tunable fluorescence has already been demonstrated in biological applications for sensing and drug delivery. Additional chemical processing and modification should continue to progress towards this end. Solution-processed organic devices requiring electrochemical stability, chemical functionality and flexible transparent conductors will benefit from continued progress towards the development of more efficient reduction treatments for GO to improve its optoelectronics properties.

From the point of view of devices, fluorescence over a wide range of wavelengths along with solution processability of GO offers possibilities for incorporation into blue light-emitting diodes, white light emission for solid-state lighting and display applications on flexible platforms. The initial quantum efficiency values for fluorescence reported in the literature are promising. More fundamental measurements on suspended samples to eliminate the influence of the surrounding medium are required to isolate the exact fluorescence mechanism so that it can be optimized and efficiencies maximized. However, for electronics applications, the realization of electroluminescence will be a key development[101]. The relatively high mobility of rGO thin-films as compared with organic electronics materials would suggest that electroluminescence in rGO is feasible. Taking advantage of fluorescence quenching in fully reduced GO, interesting applications based on charge transfer and contrast enhancement have been demonstrated. Future applications based on the exceptional quenching ability of GO should push the detection limit resolution of biological sensors beyond the current state-of-the-art. Finally, nonlinear optical effects within GO should be useful for broadband applications such as absorbers for ultrafast lasers and eye protection.

To move forward, chemists from various backgrounds will be needed to develop strategies for further tuning the properties of GO. One key area will be the integration of GO with organic molecules to make multifunctional devices. The electron affinities and spectral properties of GO and the organic molecule can both be tuned, thus allowing the design of powerful donor–acceptor pairs or charge-transfer complexes. Hybrid graphene–organic materials may combine the advantages of high carrier mobilities with greater switching capabilities, useful in plastic optoelectronics devices.

References

1. Brodie, B. C. On the atomic weight of graphite. *Phil. Trans. R. Soc. Lond. A* **149,** 249–259 (1859).
2. Park, S. & Ruoff, R. S. Chemical methods for the production of graphenes. *Nature Nanotech.* **4,** 217–224 (2009).
3. Dreyer, D. R., Park, S., Bielawski, C. W. & Ruoff, R. S. The chemistry of graphene oxide. *Chem. Soc. Rev.* **39,** 228–240 (2010).
4. Loh, K. P., Bao, Q., Ang, P. K. & Yang, J. The chemistry of graphene. *J. Mater. Chem.* **20,** 2277–2289 (2010).
5. Eda, G. & Chhowalla, M. Chemically derived graphene oxide: Towards large-area thin-film electronics and optoelectronics. *Adv. Mater.* **22,** 2392–2415 (2010).
6. Eda, G., Mattevi, C., Yamaguchi, H., Kim, H. & Chhowalla, M. Insulator to semi-metal transition in graphene oxide. *J. Phys. Chem. C* **113,** 15768–15771 (2009).
7. Yang, D. *et al.* Chemical analysis of graphene oxide films after heat and chemical treatments by X-ray photoelectron and micro-Raman spectroscopy. *Carbon* **47,** 145–152 (2009).
8. Mkhoyan, K. A. *et al.* Atomic and electronic structure of graphene-oxide. *Nano Lett.* **9,** 1058–1063 (2009).
9. Mattevi, C. *et al.* Evolution of electrical, chemical, and structural properties of transparent and conducting chemically derived graphene thin films. *Adv. Funct. Mater.* **19,** 2577–2583 (2009).
10. Gómez-Navarro, C. *et al.* Atomic structure of reduced graphene oxide. *Nano Lett.* **10,** 1144–1148 (2010).
11. Jung, I. *et al.* Reduction kinetics of graphene oxide determined by electrical transport measurements and temperature programmed desorption. *J. Phys. Chem. C* **113,** 18480–18486 (2009).
12. Kang, H., Kulkarni, A., Stankovich, S., Ruoff, R. S. & Baik, S. Restoring electrical conductivity of dielectrophoretically assembled graphite oxide sheets by thermal and chemical reduction techniques. *Carbon* **47,** 1520–1525 (2009).
13. Jung, I., Dikin, D. A., Piner, R. D. & Ruoff, R. S. Tunable electrical conductivity of individual graphene oxide sheets reduced at "low" temperatures. *Nano Lett.* **8,** 4283–4287 (2008).
14. Wang, S. *et al.* High mobility, printable, and solution-processed graphene electronics. *Nano Lett.* **10,** 92–98 (2010).
15. Kudin, K. *et al.* Raman spectra of graphite oxide and functionalized graphene sheets. *Nano Lett* **8,** 36–41 (2008).
16. Ishigami, M., Chen, J. H., Cullen, W. G., Fuhrer, M. S. & Williams, E. D. Atomic structure of graphene on SiO_2. *Nano Lett.* **7,** 1643–1648 (2007).
17. Paredes, J. I., Villar-Rodil, S., Solís-Fernández, P., Martínez-Alonso, A. & Tascón, J. M. D. Atomic force and scanning tunneling microscopy imaging of graphene nanosheets derived from graphite oxide. *Langmuir* **25,** 5957–5968 (2009).
18. Wilson, N. R. *et al.* Graphene oxide: Structural analysis and application as a highly transparent support for electron microscopy. *ACS Nano* **3,** 2547–2556 (2009).
19. Kaiser, A. B., Gómez-Navarro, C., Sundaram, R. S., Burghard, M. & Kern, K. Electrical conduction mechanism in chemically derived graphene monolayers. *Nano Lett.* **9,** 1787–1792 (2009).
20. Jung, I. *et al.* Characterization of thermally reduced graphene oxide by imaging ellipsometry. *J. Phys. Chem. C* **112,** 8499–8506 (2008).
21. Akhavan, O. The effect of heat treatment on formation of graphene thin films from graphene oxide nanosheets. *Carbon* **48,** 509–519 (2010).
22. Buchsteiner, A., Lerf, A. & Pieper, J. Water dynamics in graphite oxide investigated with neutron scattering. *J. Phys. Chem. B* **110,** 22328–22338 (2006).
23. Sun, X. *et al.* Nano-graphene oxide for cellular imaging and drug delivery. *Nano Res.* **1,** 203–212 (2008).
24. Eda, G. & Chhowalla, M. Graphene-based composite thin films for electronics. *Nano Lett.* **9,** 814–818 (2009).
25. He, H. Y., Klinowski, J., Forster, M. & Lerf, A. A new structural model for graphite oxide. *Chem. Phys. Lett.* **287,** 53–56 (1998).
26. Lerf, A., He, H., Forster, M. & Klinowski, J. Structure of graphite oxide revisited. *J. Phys. Chem. B* **102,** 4477–4482 (1998).
27. Cai, W. *et al.* Synthesis and solid-state NMR structural characterization of ^{13}C-labeled graphite oxide. *Science* **321,** 1815–1817 (2008).
28. Gao, W., Alemany, L. B., Ci, L. & Ajayan, P. M. New insights into the structure and reduction of graphite oxide. *Nature Chem.* **1,** 403–408 (2009).
29. Bagri, A. *et al.* Structural evolution during the reduction of chemically derived graphene oxide. *Nature Chem.* **2,** 581–587 (2010).
30. Li, J.-L. *et al.* Oxygen-driven unzipping of graphitic materials. *Phys. Rev. Lett.* **96,** 176101 (2006).
31. Wang, S. *et al.* Room-temperature synthesis of soluble carbon nanotubes by the sonication of graphene oxide nanosheets. *J. Am. Chem. Soc* **131,** 16832–16837 (2009).
32. Lu, J. *et al.* One-pot synthesis of fluorescent carbon nanoribbons, nanoparticles, and graphene by the exfoliation of graphite in ionic liquids. *ACS Nano* **3,** 2367–2375 (2009).
33. Pan, D., Zhang, J., Li, Z. & Wu, M. Hydrothermal route for cutting graphene sheets into blue-luminescent graphene quantum dots. *Adv. Mater.* **22,** 734 -738 (2010).
34. Jian-Hao, C., Cullen, W. G., Jang, C., Fuhrer, M. S. & Williams, E. D. Defect scattering in graphene. *Phys. Rev. Lett.* **102,** 236805 (2009).
35. Kim, K. *et al.* Electric property evolution of structurally defected multilayer graphene. *Nano Lett.* **8,** 3092–3096 (2008).
36. Chipman, A. A commodity no more. *Nature* **449,** 131–131 (2007).
37. Eda, G. *et al.* Transparent and conducting electrodes for organic electronics from reduced graphene oxide. *Appl. Phys. Lett.* **92,** 233305 (2008).
38. Wu, J. *et al.* Organic solar cells with solution-processed graphene transparent electrodes. *Appl. Phys. Lett.* **92,** 263302 (2008).
39. Wu, J. *et al.* Organic light-emitting diodes on solution-processed graphene transparent electrodes. *ACS Nano* **4,** 43–48 (2010).
40. Wassei, J. K. & Kaner, R. B. Graphene, a promising transparent conductor. *Mater. Today* **13,** 52 (2010).
41. Wang, X., Zhi, L. & Müllen, K. Transparent, conductive graphene electrodes for dye-sensitized solar cells. *Nano Lett.* **8,** 323–327 (2008).
42. Becerril, H. A. *et al.* Evaluation of solution-processed reduced graphene oxide films as transparent conductors. *ACS Nano* **2,** 463–470 (2008).
43. Li, D., Müller, M. B., Gilje, S., Kaner, R. B. & Wallace, G. G. Processable aqueous dispersions of graphene nanosheets. *Nature Nanotech.* **3,** 101–105 (2008).
44. Li, X. *et al.* Highly conducting graphene sheets and Langmuir–Blodgett films. *Nature Nanotech.* **3,** 538–542 (2008).
45. Hernandez, Y. *et al.* High-yield production of graphene by liquid-phase exfoliation of graphite. *Nature Nanotech.* **3,** 563–568 (2008).
46. Tung, V. C., Allen, M. J., Yang, Y. & Kaner, R. B. High-throughput solution processing of large-scale graphene. *Nature Nanotech.* **4,** 25–29 (2009).
47. Su, Q. *et al.* Composites of graphene with large aromatic molecules. *Adv. Mater.* **21,** 1–5 (2009).
48. Shin, H.-J. *et al.* Efficient reduction of graphite oxide by sodium borohydride and its effect on electrical conductance. *Adv. Funct. Mater* **19,** 1987–1992 (2009).
49. Tung, V. C. *et al.* Low-temperature solution processing of graphene-carbon nanotube hybrid materials for high-performance transparent conductors. *Nano Lett.* **9,** 1949–1955 (2009).
50. Nair, R. R. *et al.* Fine structure constant defines visual transparency of graphene. *Science* **320,** 1308 (2008).
51. Li, X. *et al.* Transfer of large-area graphene films for high-performance transparent conductive electrodes. *Nano Lett.* **9,** 4359–4363 (2009).
52. De, S. & Coleman, J. N. Are there fundamental limitations on the sheet resistance and transmittance of thin graphene films? *ACS Nano* **4,** 2713–2720 (2010).
53. Matyba, P. *et al.* Graphene and mobile ions: The key to all-plastic, solution-processed light-emitting devices. *ACS Nano* **4,** 637–642 (2010).
54. Essig, S. *et al.* Phonon-assisted electroluminescence from metallic carbon nanotubes and graphene. *Nano Lett.* **10,** 1589–1594 (2010).
55. Sun, X. *et al.* Nano-graphene oxide for cellular imaging and drug delivery. *Nano Res.* **1,** 203–212 (2008).
56. Liu, Z., Robinson, J. T., Sun, X. & Dai, H. PEGylated nano-graphene oxide for delivery of water insoluble cancer drugs. *J. Am. Chem. Soc.* **130,** 10876 (2008).
57. Luo, Z. T., Vora, P. M., Mele, E. J., Johnson, A. T. C. & Kikkawa, J. M. Photoluminescence and band gap modulation in graphene oxide. *Appl. Phys. Lett.* **94,** 111909 (2009).
58. Eda, G. *et al.* Blue photoluminescence from chemically derived graphene oxide. *Adv. Mater.* **22,** 505–509 (2009).
59. Cuong, T. V. *et al.* Photoluminescence and Raman studies of graphene thin films prepared by reduction of graphene oxide. *Mater. Lett.* **64,** 399–401 (2010).
60. Subrahmanyam, K. S., Kumar, P., Nag, A. & Rao, C. N. R. Blue light emitting graphene-based materials and their use in generating white light. *Solid State Commun.* **150,** 1774–1777 (2010).
61. Chen, J.-L. & Yan, X.-P. A dehydration and stabilizer-free approach to production of stable water dispersions of graphene nanosheets. *J. Mater. Chem.* **20,** 4328–4332 (2010).
62. Demichelis, F., Schreiter, S. & Tagliaferro, A. Photoluminescence in a-C:H films. *Phys. Rev. B* **51,** 2143 (1995).
63. Rusli, Robertson, J. & Amaratunga, G. A. J. Photoluminescence behavior of hydrogenated amorphous carbon. *J. Appl. Phys.* **80,** 2998–3003 (1996).
64. Koos, M., Veres, M., Fule, M. & Pocsik, I. Ultraviolet photoluminescence and its relation to atomic bonding properties of hydrogenated amorphous carbon. *Diamond Relat. Mater.* **11,** 53–58 (2002).
65. Lin, Y. *et al.* Visible luminescence of carbon nanotubes and dependence on functionalization. *J. Phys. Chem. B* **109,** 14779–14782 (2005).
66. Sun, Y.-P. *et al.* Quantum-sized carbon dots for bright and colorful photoluminescence. *J. Am. Chem. Soc.* **128,** 7756–7757 (2006).

67. Liu, H., Ye, T. & Mao, C. Fluorescent carbon nanoparticles derived from candle soot. *Angew. Chem. Int. Ed.* **46,** 6473–6475 (2007).
68. Zhou, J. *et al.* An electrochemical avenue to blue luminescent nanocrystals from multiwalled carbon nanotubes (MWCNTs). *J. Am. Chem. Soc.* **129,** 744–745 (2007).
69. Luo, Y. *et al.* Highly visible-light luminescence properties of the carboxyl-functionalized short and ultrashort MWNTs. *J. Solid State Chem.* **180,** 1928–1933 (2007).
70. Gokus, T. *et al.* Making graphene luminescent by oxygen plasma treatment. *ACS Nano* **3,** 3963–3968 (2009).
71. Kanemitsu, Y., Okamoto, S., Otobe, M. & Oda, S. Photoluminescence mechanism in surface-oxidized silicon nanocrystals. *Phys. Rev. B* **55,** R7375–R7378 (1997).
72. Dong, L., Joseph, K. L., Witkowski, C. M. & Craig, M. M. Cytotoxicity of single-walled carbon nanotubes suspended in various surfactants. *Nanotechnology* **19,** 255702 (2008).
73. Yang, K. *et al.* Graphene in mice: Ultrahigh in vivo tumor uptake and efficient photothermal therapy. *Nano Lett.* **10,** 3318–3323 (2010).
74. Kagan, M. R. & McCreery, R. L. Reduction of fluorescence interference in Raman spectroscopy via analyte adsorption on graphitic carbon. *Anal. Chem.* **66,** 4159–4165 (1994).
75. Treossi, E. *et al.* High-contrast visualization of graphene oxide on dye-sensitized glass, quartz, and silicon by fluorescence quenching. *J. Am. Chem. Soc.* **131,** 15576–15577 (2009).
76. Kim, J., Cote, L. J., Kim, F. & Huang, J. Visualizing graphene based sheets by fluorescence quenching microscopy. *J. Am. Chem. Soc.* **132,** 260–267 (2010).
77. Liu, Z. *et al.* Organic photovoltaic devices based on a novel acceptor material: graphene. *Adv. Mater.* **20,** 3924–3930 (2008).
78. Wang, Y., Kurunthu, D., Scott, G. W. & Bardeen, C. J. Fluorescence quenching in conjugated polymers blended with reduced graphitic oxide. *J. Phys. Chem. C* **114,** 4153–4159 (2010).
79. Dong, H., Gao, W., Yan, F., Ji, H. & Ju, H. Fluorescence resonance energy transfer between quantum dots and graphene oxide for sensing biomolecules. *Anal. Chem.* **82,** 5511–5517 (2010).
80. Xie, L., Ling, X., Fang, Y., Zhang, J. & Liu, Z. Graphene as a substrate to suppress fluorescence in resonance raman spectroscopy. *J. Am. Chem. Soc.* **131,** 9890–9891 (2009).
81. Kim, J., Kim, F. & Huang, J. Seeing graphene-based sheets. *Mater. Today* **13,** 28–38.
82. Blake, P. *et al.* Making graphene visible. *Appl. Phys. Lett.* **91,** 063124 (2007).
83. Swathi, R. S. & Sebastian, K. L. Resonance energy transfer from a dye molecule to graphene. *J. Chem. Phys.* **129,** 054703 (2008).
84. Swathi, R. S. & Sebastian, K. L. Long range resonance energy transfer from a dye molecule to graphene has (distance)$^{-4}$ dependence. *J. Chem. Phys.* **130,** 086101 (2009).
85. Ling, X. *et al.* Can graphene be used as a substrate for Raman enhancement? *Nano Lett.* **10,** 553–561 (2009).
86. Balapanuru, J. *et al.* A graphene oxide-organic dye ionic complex with DNA-sensing and optical-limiting properties. *Angew. Chem. Int. Ed.* **49,** 6549–6553 (2010).
87. Lu, C.-H., Yang, H.-H., Zhu, C.-L., Chen, X. & Chen, G.-N. A graphene platform for sensing biomolecules. *Angew. Chem. Int. Ed.* **48,** 4785–4787 (2009).
88. He, S. *et al.* A graphene nanoprobe for rapid, sensitive, and multicolor fluorescent DNA analysis. *Adv. Funct. Mater.* **20,** 453–459 (2010).
89. Chang, Y. R. *et al.* Mass production and dynamic imaging of fluorescent nanodiamonds. *Nature Nanotech.* **3,** 284–288 (2008).
90. Fu, C. C. *et al.* Characterization and application of single fluorescent nanodiamonds as cellular biomarkers. *Proc. Natl Acad. Sci. USA* **104,** 727–732 (2007).
91. Satishkumar, B. C. *et al.* Reversible fluorescence quenching in carbon nanotubes for biomolecular sensing. *Nature Nanotech.* **2,** 560–564 (2007).
92. Dedecker, P., Hofkens, J. & Hotta, J-i. Diffraction-unlimited optical microscopy. *Mater. Today* **11,** 12–21 (2008).
93. Liu, Z. B. *et al.* Nonlinear optical properties of graphene oxide in nanosecond and picosecond regimes. *Appl. Phys. Lett.* **94,** 021902 (2009).
94. Xu, Y. *et al.* A graphene hybrid material covalently functionalized with porphyrin: Synthesis and optical limiting property. *Adv. Mater.* **21,** 1275–1279 (2009).
95. Liu, Y. S. *et al.* Synthesis, characterization and optical limiting property of covalently oligothiophene-functionalized graphene material. *Carbon* **47,** 3113–3121 (2009).
96. Liu, Z. B. *et al.* Porphyrin and fullerene covalently functionalized graphene hybrid materials with large nonlinear optical properties. *J. Phys. Chem. B* **113,** 9681–9686 (2009).
97. Kumar, S. *et al.* Femtosecond carrier dynamics and saturable absorption in graphene suspensions. *Appl. Phys. Lett.* **95,** 191911 (2009).
98. Bao, Q. *et al.* Atomic-layer graphene as a saturable absorber for ultrafast pulsed lasers. *Adv. Funct. Mater.* **19,** 3077–3083 (2009).
99. Bao, Q. *et al.* Graphene–polymer nanofiber membrane for ultrafast photonics. *Adv. Funct. Mater.* **20,** 782–791 (2010).
100. Wang, J., Hernandez, Y., Lotya, M., Coleman, J. N. & Blau, W. J. Broadband nonlinear optical response of graphene dispersions. *Adv. Mater.* **21,** 2430–2435 (2009).
101. Fan, F. R. F., Park, S., Zhu, Y. W., Ruoff, R. S. & Bard, A. J. Electrogenerated chemiluminescence of partially oxidized highly oriented pyrolytic graphite surfaces and of graphene oxide nanoparticles. *J. Am. Chem. Soc.* **131,** 937–939 (2009).

Acknowledgements

K.P.L. is supported by the NRF-CRP grant 'Graphene Related Materials and Devices', R-143-000-360-281. M.C. acknowledges funding from the US NSF CAREER Award (ECS 0543867). G.E. and M.C. also acknowledge financial support from the Center for Advanced Structural Ceramics (CASC) at Imperial College London. G.E. acknowledges the Royal Society for the Newton International Fellowship. M.C. acknowledges support from the Royal Society through the Wolfson Merit Award.